Naval Research Laboratory
Washington, DC 20375-5000

NRL Memorandum Report 6453

Efficient Second Harmonic Conversion of Broadband High-Peak-Power Nd:Glass Laser Radiation Using Large-Aperture KDP Crystals in Quadrature

M. PRONKO, R. LEHMBERG, S. OBENSCHAIN, C. PAWLEY, C. MANKA AND R. ECKARDT*

Plasma Physics Division

**Stanford University*
W.W. Hansen Laboratories of Physics
Stanford, California 94305-4085

June 23, 1989

SECURITY CLASSIFICATION OF THIS PAGE

REPORT DOCUMENTATION PAGE

Form Approved
OMB No. 0704-0188

1a. REPORT SECURITY CLASSIFICATION UNCLASSIFIED	1b. RESTRICTIVE MARKINGS
2a. SECURITY CLASSIFICATION AUTHORITY	3. DISTRIBUTION / AVAILABILITY OF REPORT Approved for public release; distribution unlimited.
2b. DECLASSIFICATION / DOWNGRADING SCHEDULE	
4. PERFORMING ORGANIZATION REPORT NUMBER(S) NRL Memorandum Report 6453	5. MONITORING ORGANIZATION REPORT NUMBER(S)
6a. NAME OF PERFORMING ORGANIZATION Naval Research Laboratory 6b. OFFICE SYMBOL (If applicable) Code 4731	7a. NAME OF MONITORING ORGANIZATION
6c. ADDRESS (City, State, and ZIP Code) Washington, DC 20375-5000	7b. ADDRESS (City, State, and ZIP Code)
8a. NAME OF FUNDING / SPONSORING ORGANIZATION Department of Energy 8b. OFFICE SYMBOL (If applicable)	9 PROCUREMENT INSTRUMENT IDENTIFICATION NUMBER
8c. ADDRESS (City, State, and ZIP Code)	10 SOURCE OF FUNDING NUMBERS PROGRAM ELEMENT NO PROJECT NO 92 DE-AI08 79-DE-400 TASK NO WORK UNIT ACCESSION NO
11. TITLE (Include Security Classification) Efficient Second Harmonic Conversion of Broadband High-Peak-Power Nd:Glass Laser Radiation Using Large-Aperture KDP Crystals in Quadrature	
12. PERSONAL AUTHOR(S) Pronko, M.S., Lehmberg, R., Obenschain, S.P., Pawley, C., Manka, C. and Eckardt,* R.	
13a. TYPE OF REPORT 13b. TIME COVERED FROM _____ TO _____ 14. DATE OF REPORT (Year, Month, Day) 1989 June 23 15. PAGE COUNT 42	
16 SUPPLEMENTARY NOTATION *Stanford University, W.W. Hansen Laboratories of Physics, Stanford, California 94305-4085	
17 COSATI CODES FIELD / GROUP / SUB-GROUP	18 SUBJECT TERMS (Continue on reverse if necessary and identify by block number) Second harmonic conversion efficiency KDP crystals Broadband Nd: glass laser Induced spatial incoherence

19 ABSTRACT (Continue on reverse if necessary and identify by block number)

We have investigated the second harmonic conversion efficiency of broadband Nd: glass laser light ($\Delta\nu/c$ < 30 cm^{-1} FWHM). Using two KDP crystals in a quadrature arrangement we obtained energy conversion efficiencies ~ 55% with an initial bandwidth for the fundamental of ($\Delta\nu/c$ ~ 17 cm^{-1} FWHM. For these conditions, we observed a modest increase (~ 70%) in the harmonic bandwidth (FWHM) relative to the fundamental. The usual theory of three-wave mixing in dispersive birefringent nonlinear crystals is extended to describe the broadband harmonic conversion process; the generalized theory includes the statistical properties of the light and phase mismatch effects on the spectral components in the complex field amplitudes. Good agreement is shown between the code calculations and the measurements.

20 DISTRIBUTION / AVAILABILITY OF ABSTRACT ☒ UNCLASSIFIED/UNLIMITED ☐ SAME AS RPT ☐ DTIC USERS	21 ABSTRACT SECURITY CLASSIFICATION UNCLASSIFIED
22a NAME OF RESPONSIBLE INDIVIDUAL Mark S. Pronko	22b TELEPHONE (Include Area Code) (202) 767-3299 22c OFFICE SYMBOL Code 4731

DD Form 1473, JUN 86 *Previous editions are obsolete* SECURITY CLASSIFICATION OF THIS PAGE

S/N 0102-LF-014-6603

CONTENTS

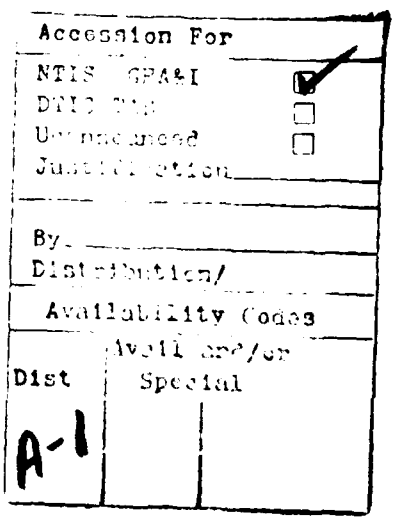

EFFICIENT SECOND HARMONIC CONVERSION OF BROADBAND HIGH-PEAK-POWER Nd:GLASS LASER RADIATION USING LARGE-APERTURE KDP CRYSTALS IN QUADRATURE

I. Introduction

Large Nd:glass laser systems have been developed as tools for laser fusion research. Recent laser-matter interaction experiments have shown that a laser wavelength shorter than one micron is required for efficient target coupling and suppression of some laser-plasma instabilities [1]-[5]. For directly driven fuel pellets, one also requires nearly uniform illumination to produce the highly-symmetric ablation pressure necessary for high gain. Estimates for this symmetry suggest that it must be better than one or two percent [6],[7]. These requirements have stimulated the development of techniques to improve focal uniformity [8]-[11] and efficiently produce shorter wavelength light by harmonic conversion [12]-[18].

One of the more promising beam smoothing techniques, Induced Spatial Incoherence (ISI) [8],[19], requires laser radiation with a short coherence time ($\tau < 2$ ps) and therefore a broad bandwidth ($\Delta\upsilon/c > 15$ cm^{-1}). Bandwidths of up to 30 cm^{-1} are readily achievable in Nd:glass laser systems in the spectral region near one micron. Evaluation of the ISI technique at shorter wavelength using a Nd:glass laser system requires a harmonic conversion process that also

Manuscript approved April 13, 1989.

maintains broad bandwidth. Here, we report the production of broadband 527-nm has several advantages over the conventional single Type II crystal. In a single Type II crystal, birefringence limits the conversion efficiency by creating a group velocity mismatch between the two orthogonal components of the fundamental. The quadrature configuration compensates for this mismatch because the transverse projections of the two crystal's principle axes are orthogonal, as shown in Fig. 1. Hence, the fundamental component that is polarized along the slow axis in the first crystal will be polarized along the fast axis in the second. This arrangement also retains the major advantages of Type II operation (i.e., a wide input intensity range over which conversion is high [18] and a relatively high tolerance to small angular misalignments and beam divergence). Furthermore, harmonic back-conversion is minimized because the second harmonic light produced in the first crystal is not at the correct polarization for interaction in the second.

A theoretical model which simulates the broadband conversion process is described in Section II. Using this model, we calculated the conversion efficiency and spectral properties of the harmonically generated radiation for two specific input bandwidths. Details of the experimental arrangement are presented in Section III. The experimental results are presented in Section IV where reasonable agreement with the numerical calculations is also shown.

II. Theory of Broadband Harmonic Conversion

Broadband harmonic conversion can be described by the usual theory of three wave mixing in dispersive birefringent nonlinear crystals [20]. Each of the colinearly propagating waves $\xi_1(z,t)$, $\xi_2(z,t)$, $\xi_3(z,t)$ can be written in the form

$$\xi_n(z,t) = {}^1/_2 E_n(z,t)\exp[i(k_n z - \omega_n t)] + \text{c.c.} , \tag{1}$$

where the spatial and temporal angular carrier frequencies are chosen to satisfy the exact phase-matching conditions

$$k_1 + k_2 - k_3 = 0 , \qquad \omega_1 + \omega_2 - \omega_3 = 0 , \tag{2}$$

and the complex amplitudes $E_n(z,t)$ are assumed to be slowly-varying on the scale of k_n^{-1} and ω_n^{-1}. For the broadband case, these amplitudes must account for the statistical properties of the light, plus any phase mismatch effects on spectral components that are detuned from the carrier frequencies.

The coupled amplitude equations are [21], [22]

$$(\partial/\partial z + a_1\partial/\partial t + ib_1\partial^2/\partial t^2 + \beta_1)E_1 = - \omega_1 C E_3 E_2^* , \tag{3a}$$

$$(\partial/\partial z + a_2\partial/\partial t + ib_2\partial^2/\partial t^2 + \beta_2)E_2 = - \omega_2 C E_3 E_1^* , \tag{3b}$$

$$(\partial/\partial z + ib_3\partial^2/\partial t^2 + \beta_3)E_3 = \omega_3 C E_1 E_2 \ , \qquad (3c)$$

where $a_n \equiv v_{gn}^{-1} - v_{g3}^{-1}$, $v_{gn}^{-1} \equiv \partial k_n/\partial\omega_n$ is the inverse group velocity of the nth wave, $b_n \equiv {}^1/_2\partial^2 k_n/\partial\omega_n^2$ accounts for the group velocity dispersion, β_n is the linear loss term, and C is the nonlinear coupling constant. If the amplitudes are scaled as $|E_n|^2 \equiv I_n$, where I_n is the intensity in W/cm^2 and the lengths and velocities in equations (3) are in units of cm and cm/s respectively, then the coupling constant is

$$C = (2 \times 10^6/\epsilon_o c^3 n_1 n_2 n_3)^{1/2}(d/\epsilon_o)\sin(m\theta_m) \ ,$$

where ϵ_o is the permittivity of free space in MKS units, c is the velocity of light, and n_n are the refractive indices. The nonlinear optical coefficient is defined such that for KDP d/ϵ_o = 0.39 pm/V. The phase matching angle is θ_m; for Type I phase matching m = 1, and for Type II m = 2. Equations (3) describe the interaction as seen by an observer moving along with the E_3 amplitude. For most cases of interest, the contributions due to group velocity dispersion are small in comparison to the other terms.

In second harmonic conversion, $E_1 \rightarrow E_{\omega x}$ and $E_2 \rightarrow E_{\omega y}$ represent orthogonal spatial components of the fundamental amplitude E_ω ($\omega_1 = \omega_2 \equiv \omega$), while $E_3 \rightarrow E_{2\omega}$ describes the harmonic ($\omega_3 \equiv 2\omega$). The limitations on 2ω conversion imposed by finite optical bandwidth can be easily illustrated in the limit of negligible pump depletion $|E_{2\omega}| \ll |E_\omega|$. If one also ignores the small absorption and group velocity dispersion effects, then the mixing equations reduce to

$$(\partial/\partial z + a_1\partial/\partial t)E_{\omega x} \simeq 0 \ , \tag{4a}$$

$$(\partial/\partial z + a_2\partial/\partial t)E_{\omega y} \simeq 0 \ , \tag{4b}$$

$$\partial E_{2\omega}/\partial z \simeq 2\omega C E_{\omega x}E_{\omega y} \ . \tag{4c}$$

For a crystal of thickness L and the usual boundary condition $E_{2\omega} = 0$ at $z = 0$, the solution is

$$E_{2\omega}(t) = 2\omega C \int_0^L E_{\omega x}(t - a_1 z)E_{\omega y}(t - a_2 z)dz \ . \tag{5}$$

It is instructive to first consider the case where the fundamental is a monochromatic wave whose actual frequency is detuned from ω by some small amount $\delta\omega$; i.e., $E_{\omega j}(t) \to A_j \exp(-i\delta\omega t)$, where $A_j \to A_x$, A_y are constants. Then

$$E_{2\omega}(t) = 2\omega C A_x A_y L \exp[-2i\delta\omega(t - 1/2\Delta\upsilon_{cr})]\,\mathrm{sinc}(\delta\omega/\Delta\upsilon_{cr}) \ , \tag{6}$$

where $\mathrm{sinc}(x) \equiv \sin(x)/x$ and

$$\Delta\upsilon_{cr} \equiv \frac{2/L}{a_1 + a_2} = \frac{1/L}{1/2(v_{g1}^{-1} + v_{g2}^{-1}) - v_{g3}^{-1}} \tag{7}$$

is the frequency bandpass ($\Delta\omega_{cr}/2\pi$) of the crystal in the low conversion limit [23].

In the broadband case, the incident fundamental is modeled by quasi-stationary chaotic noise [24]. Its spectrum is comprised of many randomly-phased modes of total bandwidth $\Delta\nu_F$ centered around $\omega/2\pi$. Thus $E_\omega(t)$ is a stochastic function characterized by a coherence time $t_c = 1/\Delta\nu_F$ much shorter than the laser pulse duration. Applying these considerations to expression (5), one observes that if $|a_1|L$, $|a_2|L \ll t_c$, then $E_{2\omega}(t)$ is given by the phase-matched result $2\omega C E_{\omega x}(t)E_{\omega y}(t)L$. However, if either $|a_1|L$ or $|a_2|L$ become comparable to t_c, the integrand can undergo a phase shift within the (0,L) interval, resulting (on the average) in lower harmonic conversion. The interpretation of these results is straightforward in Type I operation, where $a_1 = a_2 \equiv a_I$. According to expression (7), the criterion $|a_I|L \ll t_c$ then reduces to

$$\Delta\nu_F \ll \Delta\nu_{cr} \; ; \tag{8}$$

i.e., the optical bandwidth must be much less than the crystal bandpass. For 1.054 μm light in KDP, we find $a_I = 0.0529$ ps/cm, thus giving $\Delta\nu_{cr}/c \simeq 630$ cm^{-1} (280 cm^{-1} FWHM) for L = 1 cm. Type I operation offers the advantages of simplicity and broad spectral bandpass, but the angular tolerance and the intensity range over which the conversion remains high both tend to be relatively narrow in comparison to those of Type II operation.

In Type II operation, the conversion may be limited more by the crystal's birefringence than by its bandpass. Consider for example Type II operation of KDP at 1.054 μm. If $E_{\omega x}$ lies along the o axis and $E_{\omega y}$ lies in the oe plane, then $a_1 \to a_o = 0.5539$ ps/cm and $a_2 \to a_e = -0.7669$ ps/cm. Expression (7) then gives $\Delta\nu_{cr}/c \simeq 313$ cm^{-1} (138 cm^{-1} FWHM) for L = 1 cm, which suggests that high

conversion could be achieved in a single crystal with the 20 cm^{-1} to 30 cm^{-1} optical bandwidths available from Nd:glass lasers. However, criterion (8) is no longer sufficient to ensure high conversion because a_1 and a_2 are of opposite sign. An observer moving along z with the $E_{2\omega}$ amplitude (as described in Eq. (5)) would see $E_{\omega x}$ retarded by a_o ps/cm, while $E_{\omega y}$ advanced by $|a_e|$ ps/cm. These amplitudes can remain correlated, thus allowing the integrand of Eq. (5) to remain constant along z, only if the condition

$$t_c/L > a_o + |a_e| = 1.321 \text{ ps/cm} \tag{9}$$

is satisfied. In a single crystal, this criterion will effectively limit the intensity conversion to ~ 50% at bandwidths of 20 cm^{-1} to 30 cm^{-1}.

Higher conversions can be achieved without sacrificing the advantages of Type II operation by using the quadrature configuration [18] shown in Fig. 1. The first crystal is oriented as described above. At the output, $E_{\omega x}$ is retarded by a_oL while $E_{\omega y}$ is advanced by $|a_e|L$. This crystal can convert 30% to 50% of the light at bandwidths of 20 cm^{-1} 30 cm^{-1} if $(a_o + |a_e|)L \sim t_c$. In the second crystal the optic axis is rotated 90° around the propagation direction, thus interchanging the transverse projections of the o and e axes. The amplitude $E_{\omega x}$ will now begin to advance at the rate $|a_e|$ ps/cm, while $E_{\omega y}$ retards at the rate a_o ps/cm. If this crystal has a thickness $L' \simeq 2L$, then $E_{\omega x}$ and $E_{\omega y}$ will be back in step around its midplane, and its harmonic contribution $E_{2\omega}'$ can be generated efficiently along most of its path. The harmonic contribution $E_{2\omega}$ generated by the first crystal is orthogonal to $E_{2\omega}'$. Thus $E_{2\omega}$ is not phase-matched in the second crystal, and will propagate through it with only the

linear losses $\kappa E_{2\omega}$ due to absorption and Fresnel reflection. The net intensity conversion is then given by

$$\eta = \frac{(1 - \kappa^2)\langle I_{2\omega}\rangle + \langle I_{2\omega}'\rangle}{\langle I_{\omega}(0,t)\rangle} , \tag{10}$$

where $\langle I_n\rangle \equiv \langle |E_n|^2\rangle$ is the intensity of the nth wave averaged over times much longer than t_c and $\langle I_{\omega}(0,t)\rangle$ is the total fundamental $\langle I_{\omega x}\rangle + \langle I_{\omega y}\rangle$ incident at the first crystal. Using low loss crystals and high quality AR coatings, one can achieve intensity conversions greater than 75% with output bandwidths of $\sim 30\ cm^{-1}$.

Broadband 2ω conversion has been modeled in detail by use of a numerical code FAST2F to integrate Eqs. (3). The temporal variation is handled by fast Fourier transform techniques similar to those described elsewhere [21],[25]. If $\tilde{E}_n(z,\Omega)$ is the Fourier transform of $E_n(z,t)$, i.e.

$$\tilde{E}_n(z,\Omega) \equiv T_F\{E_n(z,t)\} , \quad E_n(z,t) = T_F^{-1}\{\tilde{E}_n(z,\Omega)\} , \tag{11}$$

then Eqs. (3) take the general form

$$(\partial/\partial z - ia_n\Omega - ib_n\Omega^2 + \beta_n)\tilde{E}_n = T_F\{M_n\} , \tag{12}$$

where M_n is the mixing term for the nth wave. (For example, $M_1 \equiv -\omega_1 C E_3 E_2^*$.) The group velocity terms, which could cause a rapid variation at larger values of Ω, are removed from the integration by using the unitary transformations

$$\bar{E}_n(z,\Omega) \equiv \bar{E}_n' \exp(ia_n\Omega + ib_n\Omega^2) \tag{13}$$

to rewrite Eq. (12) in the "interaction representation,"

$$(\partial/\partial z + \beta_n)\bar{E}_n' = \exp(-ia_n\Omega - ib_n\Omega^2)T_F\{M_n\}. \tag{14}$$

Equations (14) are then integrated by a predictor-corrector technique, using Eqs. (11) and (13) at each new point along z. This algorithm was benchmarked against the well-known analytic result [26] for monochromatic light detuned from the exact phase matching frequency; the agreement was better than 1% over a wide range of conversion efficiencies.

FAST2F calculates the total harmonic conversion and the spectral and statistical properties of the 2ω light; it can be configured for either Type I or quadrature Type II operation. It also evaluates the correlation between the harmonic amplitudes generated by two correlated but physically separate input beams differing only in their intensities. With that data, one can assess the possible deterioration of transverse coherence (and hence beam quality) that can sometimes occur when a crystal is strongly driven by a spatially nonuniform input intensity [27]. For the simulations reported here, these harmonic amplitudes remained correlated to better than 90%. The crystal parameters used for the Type II simulations are listed in Table I. All of the refractive index and group velocity parameters are taken from data of Zernike [28]; the reflectivities of the AR coatings (described in the next section) and the internal loss coefficients were specified by their respective manufacturers [29].

The incident fundamental was modeled by an array of Gaussian-distributed random complex numbers whose power spectrum envelope matched the time-integrated laser spectra measured in the experiment (see Section IV). This resulted in stochastic temporal behavior characterized by coherence time $t_c = 1/\Delta\nu_F$, which remained statistically-stationary over the entire calculation range $(0,T) >> t_c$. In order to avoid aliasing behavior, the intensity was terminated within a short transition interval t_{tr} ($t_c < t_{tr} << T$) at both ends of the calculation range. For the simulations reported here, the width of the remaining (statistically-stationary) interval was $T_s = 580$ ps, while the coherence times were typically ~ 1 ps. All intensity averages, such as those used in Eq. (10), were evaluated over this interval.

Fig. 2 shows a typical simulation of the stochastic temporal behavior, power spectrum, and autocorrelation function for the incident fundamental where the intensity averaged over the sampling interval is 1 GW/cm^2. In the spectral plot, the power is averaged over ± 1 cm^{-1} in order to roughly model the limited resolution of the spectrograph used to make the measurements. The 2ω simulations were carried out assuming that the crystals are phase-matched to the center of the incident fundamental; hence the zero frequency was chosen to lie at the centroid of this spectrum. The estimated FWHM width of the spectrum is 17 cm^{-1}. From the autocorrelation plot, we calculate a coherence time $t_c \simeq 2$ ps; the corresponding spectral width $1/t_c \rightarrow 16.7$ cm^{-1} is consistent with the estimated FWHM.

Figs. 3 and 4 show the calculated temporal behavior, spectra, and autocorrelation functions for the 2ω generated by each of the quadrature

crystals. In this example, the first crystal converted ~ 43% of the incident fundamental (described in Fig. 2), while the second converted an additional ~ 29%. The FWHM bandwidths estimated from the spectra are again consistent with the effective values $1/t_c$ found from the autocorrelation functions. (i.e., 26 cm^{-1} FWHM vs. $1/t_c \rightarrow 28$ cm^{-1} for the first crystal, and 35 cm^{-1} FWHM vs. $1/t_c \rightarrow 33$ cm^{-1} for the second.) The bandwidths from the first crystal generally remained within 1.4 to 1.6 times that of the fundamental, but the spectra from the second crystal broadened significantly at higher intensities, as shown in Fig. 5. This appears to result from a broadening of the fundamental by the conversion process in the first crystal; at higher intensities that process will preferentially deplete the central portion of the fundamental spectrum. In practice, this effect will result in only a modest broadening of the total harmonic spectrum because most of the conversion at high intensities occurs in the first crystal. The harmonic components generated by each crystal are orthogonally polarized, so the total second harmonic spectrum may be calculated by simply adding the individual spectral intensities. Fig. 6 shows the calculated total harmonic spectrum for an incident fundamental with 1 GW/cm^2 average intensity and 17 cm^{-1} bandwidth. At this intensity, where the 2ω spectrum is dominated by high conversion in the first crystal, the estimated FWHM bandwidth is 28 cm^{-1}.

Fig. 7 shows calculated intensity conversion efficiencies for two incident fundamental bandwidths. The results were evaluated using expression (10), with all intensities averaged over the 580 ps interval discussed above. In order to estimate the accuracy of the results, we ran the simulations for the 0.5 GW/cm^2 and 2.0 GW/cm^2 points using four statistically-independent realizations of the

random fundamental amplitude at the input. The RMS deviation from the average values was ~ 0.5% for the total conversion (solid curves) and ~ 0.7% for the first crystal (dashed curves). It is apparent from these curves that quadrature conversions are not only higher than those of a single crystal, but they also remain high over a much wider range of input intensities. In fact, this feature is one of the most important advantages of the quadrature configuration [18]. The curves also show that there is little penalty for using the broader bandwidth (27 cm^{-1}) fundamental to achieve output bandwidths in excess of 35 cm^{-1}. For the 2.5 ns (FWHM) pulses used in the experiment, the peak intensity was limited to ~ 1 GW/cm^2 by the ~ 5 J/cm^2 damage threshold of the crystals. The curves indicate that higher conversions should be possible with the high damage threshold crystals currently under development at Osaka University [30].

III. Experimental Apparatus

The fundamental light for the conversion efficiency measurements was produced by the PHAROS III laser system. The laser (see Fig. 8) is an image-relayed, Nd-doped phosphate glass system developed at NRL to study laser-matter interaction. The laser produces up to ~ 800 J per beam of 1.054 μm light at the output of the final 15-cm clear aperture disc amplifier. The beam is expanded by a telescope to a 20-cm diameter before frequency conversion. For this investigation, the maximum energy incident on the crystals was ~ 500 J in a 2.5 ns pulse with typical FWHM bandwidths of either ~ 17 cm^{-1} or ~ 27 cm^{-1}. The corresponding maximum peak intensity averaged across the beam was ~ 1 GW/cm^2.

The bandwidth of the laser system was varied by changing the bandwidth of the oscillator. The broad fluorescence linewidth of the Nd-phosphate glass amplifier used in the oscillator allows many longitudinal modes to exist in the 60-cm long cavity. Our oscillator (shown in Fig. 9) produces a 40-ns long pulse (FWHM) in the TEM_{oo} mode. The oscillator can be operated with or without the angle-tuned etalon shown in the figure. A typical output spectrum with an estimated FWHM of 15 cm^{-1} is shown in Fig. 10a where the oscillator was operated without the intra-cavity etalon. The structure in the spectrum is attributed to weak etalon-like behavior of the stacked-plate polarizer. Broader bandwidths were obtained using a 0.10-mm thick etalon with a reflectivity of 1.7% per surface oriented in the cavity to suppress the center of the output spectrum producing the lineshape shown in Fig. 10b. A wide variety of spectral lineshapes can in fact be produced using various combinations of etalons and by controlling the round-trip cavity gain.

A nominal 2.5-ns long Gaussian-like pulse was sliced from the peak of the longer oscillator pulse using two Pockel's cells in series driven by a fast (~ 1 ns risetime), high-voltage Krytron pulse generator. The contrast ratio of the Pockel's cell pulse slicer is greater than 10^6. The temporally shaped pulse is then amplified before being split into three equal intensity beams for delivery to the large-aperture amplifier chains. Each amplifier chain consists of a double-passed 45-mm diameter rod amplifier and three disc amplifiers ranging in clear aperture from 66 mm to 150 mm. Image-relaying telescopes transport and expand the beam from an initial 45-mm diameter to the final 150-mm

diameter. In addition, Pockel's cells and Faraday Rotators are used for interstage isolation and protection from target backscatter.

The degree of polarization, spatial quality and divergence of the fundamental beam can significantly effect the harmonic conversion efficiency. A major concern in high-peak-power glass laser systems is the effect on beam quality of high-intensity spatial fluctuations enhanced by nonlinear phase shifts. In addition to damaging optics, these effects may also cause intensity dependent depolarization and beam break-up, as has been observed elsewhere [31],[32]. Image-relaying and spatial filtering can ameliorate but not eliminate these problems. PHAROS III is image-relayed but not tightly spatially filtered; thus there was some concern that beam quality might limit the harmonic conversion efficiency. An attempt to measure the depolarization of the beam was made using a large-aperture thin-film polarizer and calorimeters to monitor the incident and rejected energy. The results were limited by the resolution and accuracy of the calorimeters, but they indicate that the beam is linearly polarized to better than a few percent. The spatial quality of the beam was assessed by imaging an attenuated reflection of the beam onto Polaroid positive/negative film. To calibrate the film, the beam was passed through a wedged rattle plate to produce multiple images on the film which differed in intensity by a known amount. The negatives were scanned through the center line with a densitometer to produce film density curves. The resulting curves are nearly linearly proportional to the time-integrated intensity. A typical profile is shown in Fig. 11. The densitometer scan taken along one diameter shows a nominally flat-topped intensity distribution with local spatial nonuniformities of less than

± 50% about the average. The divergence of the beam was inferred from the diffraction pattern produced by passing the beam through a mask containing an array of circular apertures. Using this method, we measured the maximum full-angle divergence of the beam to be ~ 130 μrad. Measurements of the focal diameter indicated that the beam was ~ 7 times the diffraction limit. We concluded from these results that the beam was of adequate quality to perform the conversion efficiency measurements without any additional effort to improve it.

The quadrature harmonic conversion assembly is a monolithic structure consisting of an aluminum frame in which two 25-cm square KDP crystals are mounted. The thicknesses of the first and second crystals are 1.0 cm and 2.5 cm, respectively. Both of the crystals are dual-wavelength, anti-reflection coated on both sides using a Sol-Gel process [33]. The surface reflectivity using this process is typically ~ 2% per surface at 1ω and ~ 1% per surface at 2ω [34]. Direct application of the coating to the crystal surface alleviates the Raman scattering problem that can occur when index matched fluid cells are used [15]. The crystals and their mounting frame were precision machined so that the optimum propagation axes through the crystals are within 50 μrad of each other when mounted in the holder.

IV. Experimental Results

The measurements were made with the diagnostic arrangement shown in Fig. 12. Volume absorbing calorimeters were used to measure the energy at both the

fundamental and second harmonic wavelengths. Because the energy measurement is time integrated and harmonic conversion is intensity dependent, both the temporal pulse shape and the spatial profile of the fundamental are required to evaluate the energy conversion efficiency. The temporal profile was measured with a silicon PIN diode which has an impulse response of ~ 300 ps. Measurement of the spatial profile was described in the previous section. Within the resolution of the measurements, neither the temporal pulse shape nor the spatial profile varied appreciably from shot to shot. Thus to evaluate the conversion efficiency, a generic temporal pulse shape and spatial profile were convolved with the appropriate theoretical data presented in Fig. 7. This results in energy conversion efficiency data expressed as a function of the incident energy for a specific temporal pulse shape and spatial profile. In Fig. 13, this data is compared to energy conversion measurements for both fundamental bandwidth cases. These results describe the external conversion efficiency of the crystal pair. (i.e., no corrections were made for crystal absorption or Fresnel losses in the experimental data, but were included in the theory.) From the figure, one can see good agreement between theory and experiment. Energy conversion efficiencies of ~ 55% were observed for laser pulse energies of ~ 500 J for the 17 cm^{-1} bandwidth. The conversion efficiency decreased by ~ 15% (from ~ 55% to ~ 47% at ~ 500 J) when the bandwidth was increased by ~ 60%. For comparison, a 15% to 20% increase in the efficiency (relative to the 17 cm^{-1} bandwidth case) was observed when a time-bandwidth limited oscillator was used with the laser.

The time-integrated spectra were measured with two 0.25-m spectrographs having resolutions of 0.05 nm and 0.025 nm for the fundamental and second harmonic, respectively. Typical spectral data are presented in Figs. 14 and 15.

Propagation of broadband radiation through a glass amplifier is complicated by the limited bandpass of the glass and self-phase modulation due to the nonlinear index. The former tends to narrow the spectral width while the latter broadens it. For our operating conditions, it is not known whether (or to what degree) these phenomena are contributing to spectral modification; however, comparison of the fundamental spectra to the corresponding oscillator spectra presented in Fig. 10 shows that these operating conditions allowed propagation through the glass amplifiers with little effect on the spectral shape. The second harmonic spectra in each case show an increase in bandwidth by a factor of 1.5 to 1.6 compared to the fundamental (consistent with the calculations presented in Section II). For the narrower bandwidth case, one finds the estimated experimental width of ~ 29 cm^{-1} for the second harmonic to agree well with the calculated value of ~ 28 cm^{-1}; differences in fine structure are due to different statistical realizations, averaging times (2.5 ns vs. the theoretical value of 580 ps) and limited resolution in the measurement.

V. Conclusions

We have shown that second harmonic light can be efficiently produced with sufficient bandwidth for ISI despite the inherent narrowband resonance of the phase-matched harmonic crystals. Conversion efficiencies of up to 55% were achieved for fundamental bandwidths of ~ 17 cm^{-1} where the incident intensities were limited by the long laser pulses. At the broader 27 cm^{-1} bandwidth, conversion efficiency was only moderately reduced. The results agree well with

code calculations, which indicate that higher conversion efficiencies are possible by increasing the fundamental input intensity.

One disadvantage to the quadrature conversion scheme is the random polarization of the harmonic beam. Some plasma instabilities are sensitive to polarization; thus, a defined polarization on target is preferred. In principle, it is possible to detune the first crystal in the quadrature configuration while maintaining adequate alignment on the second, even though the crystals are rigidly mounted together. In this situation, the second crystal becomes the primary harmonic converter while the first acts as a wave plate, thus maintaining the advantages of the quadrature configuration. Preliminary experimental results have shown that when the first crystal is detuned sufficiently to reduce its conversion efficiency by a factor of about fifteen at low power, the resulting conversion efficiency at high power is reduced only by ~ 10% for the 17-cm^{-1} bandwidth case.

Acknowledgement

The authors wish to thank N. Nocerino and J. Bone for their extensive collaboration in the design and construction of the laser system. We also thank L. Daniels and T. Peyser for their help in acquiring the experimental data and useful discussions with A. Schmitt and K. Kearney regarding the theory. The assistance of F. T. Marchi of the Lawrence Livermore National Laboratories for arranging to AR coat the crystals is appreciated. This work was supported by the US Department of Energy.

References

1. S. P. Obenschain, J. Grun, M. J. Herbst, K. J. Kearny, C. K. Manka, E. A. McLean, A. N. Mostovych, J. A. Stamper, R. R. Whitlock, S. E. Bodner, J. H. Gardner, and R. H. Lehmberg, "Laser-Target Interaction with Induced Spatial Incoherence," Phys. Rev. Lett., vol. 56, no. 26, pp. 2807-2810, June 1986.

2. A. G. M. Maaswinkel, K. Eidmann, and R. Sigel, "Comparative Reflectance Measurements on Laser-Produced Plasmas at 1.06 and 0.53 μm," Phys. Rev. Lett., vol. 42, no. 24, pp. 1625-1628, June 1979.

3. D. C. Slater, G. E. Busch, G. Charatis, R. R. Johnson, F. J. Mayer, R. J. Schroeder, J. D. Simpson, D. Sullivan, J. A. Tarvin, and C. E. Thomas, "Absorption and Hot-Electron Production for 1.05 and 0.53 μm Light on Spherical Targets," Phys. Rev. Lett., vol. 46, no. 18, pp. 1199-1202, May 1981.

4. H. Hama, K. Mima, Y. Kato, T. Uenoyama, N. Miyanaga, M. Nakai, and C. Yamanaka, "Intensity Dependence of Classical and Collective Absorption Processes in Laser Produced Plasmas at 1.053 μm and 0.527 μm," IEEE Trans. Plasma Science, vol. PS-10, no. 1, pp. 55-58, March 1982.

5. W. C. Mead, E. M. Campbell, K. G. Estabrook, R. E. Turner, W. L. Kruer, P. H. Y. Lee, B. Pruett, V. C. Rupert, K. G. Tirsell, G. L. Stradling, F. Ze, C. E. Max, and M. D. Rosen, "Laser-Plasma Interactions at 0.53 μm for Disk Targets of Varying Z," Phys. Rev. Lett. vol. 47, no. 18, pp. 1289-1292, November 1981.

6. S. E. Bodner, "Critical Elements of High Gain Laser Fusion," J. Fusion Energy, vol. 1, no. 3, pp. 221-240, 1981.

7. A. J. Schmitt, Naval Research Laboratory, private comm., 1988.

8. R. H. Lehmberg and S. P. Obenschain, "Use of Induced Spatial Incoherence for Uniform Illumination of Laser Fusion Targets," Opt. Comm., vol. 46, no.1, pp. 27-31, June 1983.

9. Y. Kato, K. Mima, M. Miyanaka, S. Aringa, Y. Kitagawa, M. Nakatsuka, and C. Yamanaka, "Random Phasing of High-Power Lasers for Uniform Target Acceleration and Plasma Instability Suppression," Phys. Rev. Lett., vol. 53, no. 11, pp. 1057-1060, September 1984.

10. X. Deng, X. Liang, Z. Chen, W. Yu, and R. Ma, "Uniform Illumination of Large Targets using a Lens Array," Appl. Opt., vol. 25, no. 3, pp. 377-381, February 1986.

11. R. H. Lehmberg and J. Goldhar, "Use of Incoherence to Produce Smooth and Controllable Irradiation Profiles with KrF Fusion Lasers," Fusion Technol., vol. 11, no. 3, pp. 532-541, May 1987.

12. M. S. Pronko, S. P Obenschain, R. H. Lehmberg, and A. N. Mostovych, "Experimental Studies on the Production of Broadband, High-Peak-Power Laser Radiation," paper presented at the Conf. on Lasers and Electro-Optics (CLEO), San Francisco, CA, June 9-13, 1986, paper THK33.

13. M. S. Pronko, S. P. Obenschain, and R. H. Lehmberg, "Experimental Studies on the Second Harmonic Generation of Broadband, High-Peak-Power Laser Radiation at 527 nm using a Quadrature Crystal Array," paper presented at the Conf. on Lasers and Electro-Optics (CLEO), Anaheim, CA, April 25-29, 1988, paper WM25.

14. P. J. Wegner, M. A. Henesian, F. T. Marchi, and D. R. Speck, "Demonstration of Efficient Full-Aperture Type I/Type II Third Harmonic Conversion on Nova," paper presented at the Conf. on Lasers and Electro-Optics (CLEO), Anaheim, CA, April 25-29, 1988, paper MF3.

15. G. J. Linford, B. C. Johnson, J. S. Hildum, W. E. Martin, K. Snyder, R. D. Boyd, W. L. Smith, C. L. Vercimak, D. Eimerl, and J. T. Hunt, "Large Aperture Harmonic Conversion Experiments at Lawrence Livermore National Laboratory," Appl. Opt., vol. 21, no. 20, pp. 3633-3643, October 1982.

16. W. Seka, S. D. Jacobs, J. E. Rizzo, R. Boni, and R. S. Craxton, "Demonstration of High Efficiency Third Harmonic Conversion of High Power Nd-Glass Laser Radiation," Opt. Comm., vol. 34,no. 3, pp. 469-473, September 1980.

17. Rutherford and Appleton Laboratories Central Laser Facility Annual Report, RL-81-040, 1981, pp. 1.19-1.22.

18. D. Eimerl, "Quadrature Frequency Conversion," IEEE J. Quantum Electron., vol. QE-23, no. 8, pp. 1361-1371, August 1987.

19. R. H. Lehmberg, A. J. Schmitt, and S. E. Bodner, "Theory of Induced Spatial Incoherence," J. Appl. Phys., vol. 62, no. 7, pp. 2680-2701, October 1987.

20. A. Yariv, Quantum Electonics, 2nd ed. New York: Wiley, 1975.

21. R. C. Eckardt and J. Rientjes, "Phase Matching Limitations of High Efficiency Second Harmonic Generation," IEEE J. Quantum Electron., vol. QE-20, no. 10, pp. 1178-1187, October 1984.

22. M. F. Becker, Y. C. Kim, S. R. Gautum and E. J. Powers, "Three-Wave Nonlinear Optical Interactions in Dispersive Media," IEEE J. Quantum Electron., vol. QE-18, no. 1, pp. 113-123, January 1982.

23. Y. S. Liu, "Spectral Phase-Matching Properties for Second Harmonic Generation in Nonlinear Crystals," Appl. Phys. Lett., vol. 31, no. 3, pp. 187-189, August 1977.

24. C. W. Helstrom, Statistical Theory of Signal Detection, 2nd ed. New York: Pergamon, 1964.

25. R. H. Lehmberg and K. A. Holder, "Numerical Study of Optical Ray Tracing in Laser-Plasma Backscatter," Phys. Rev. A, vol. 22, no. 5, pp. 2156-2170, November 1980.

26. N. Bloembergen, Nonlinear Optics. New York: Benjamin, 1965.

27. J. F. Reintjes, Naval Research Laboratory, private comm., 1988.

28. F. Zernike, "Refractive Indices of Ammonium Dihydrogen Phosphate and Potassium Dihydrogen Phosphate between 2000 A and 1.5 μ," J. Opt. Soc. Am., vol. 54, no. 10, pp. 12151220, October 1964.

29. The cystrals were grown by Clevland Crystals, Inc. and AR coated at the Lawrence Livermore National Laboratories.

30. A. Yokotani, T. Sasaki, K. Yoshida, T. Yamanaka, S. Nakai and C. Yamanaka, "Effect of the Organic Impurities in Potassium Dihydrogen Phosphate Solution on the Laser Damage Threshold of the Crystals for High Power Lasers," paper presented at the Int. Quantum Electron. Conf. (IQEC), Anaheim, CA, April 25-29, 1988, paper MP 26.

31. M. A. Henesian, R. D. Boyd, J. T. Hunt, D. R. Speck, C. D. Swift, and P. J. Wegner, "B-integral dependant ellipse rotation effects on large aperture, high-power third harmonic conversion," paper presented at the Conf. on Lasers and Electro-Optics (CLEO), San Francisco, CA, June 9-13, 1986, paper THA2.

32. W. W. Simmons, D. R. Speck, and J. T. Hunt, "Argus Laser System: Performance Summary," Appl. Opt., vol. 17, no. 7, pp. 999-1005, April 1978.

33. I. M. Thomas, "High Laser Damage Threshold Porous Silica Antireflective Coating," Appl. Opt., vol. 25, no. 9, pp. 1481-1483, May 1986.

34. F. T. Marchi, Lawrence Livermore National Laboratories, private comm., 1987.

Table 1: KDP Type II Parameters (defined in text)

Projected axis	o	e	e
Wavelength [μm]	1.054	1.054	0.527
n_n	1.49449	1.46909	1.48179
$1/v_{gn}$ [ps/cm]	50.8717	49.5509	50.3178
a_n [ps/cm]	0.5539	-0.7669	0.0
b_n [ps^2/cm]	-1.2×10^{-6}	1.1×10^{-6}	6.8×10^{-6}
$2\beta_n$ [1/cm]	0.015	0.056	0.0
Energy loss/surface	0.02	0.02	0.01

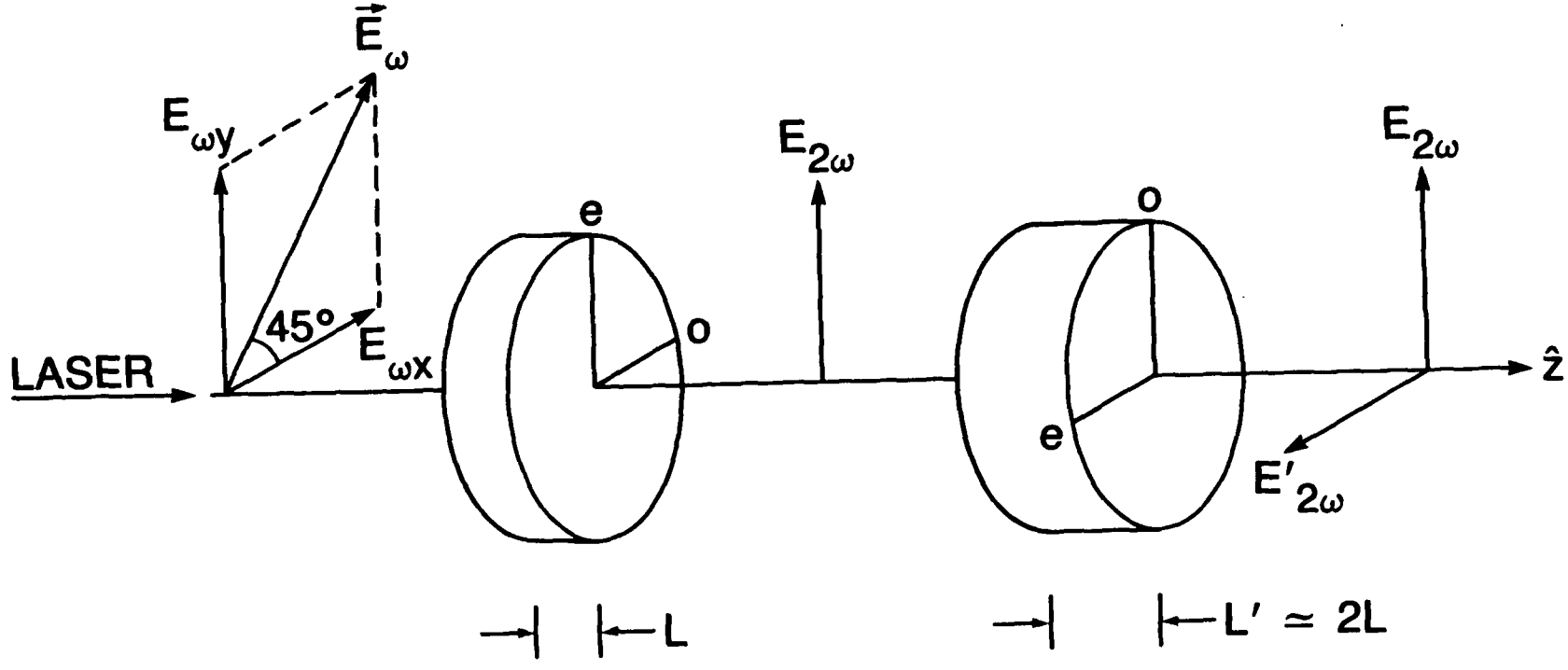

Fig. 1. Type II quadrature configuration used for the second harmonic conversion of broadband light.

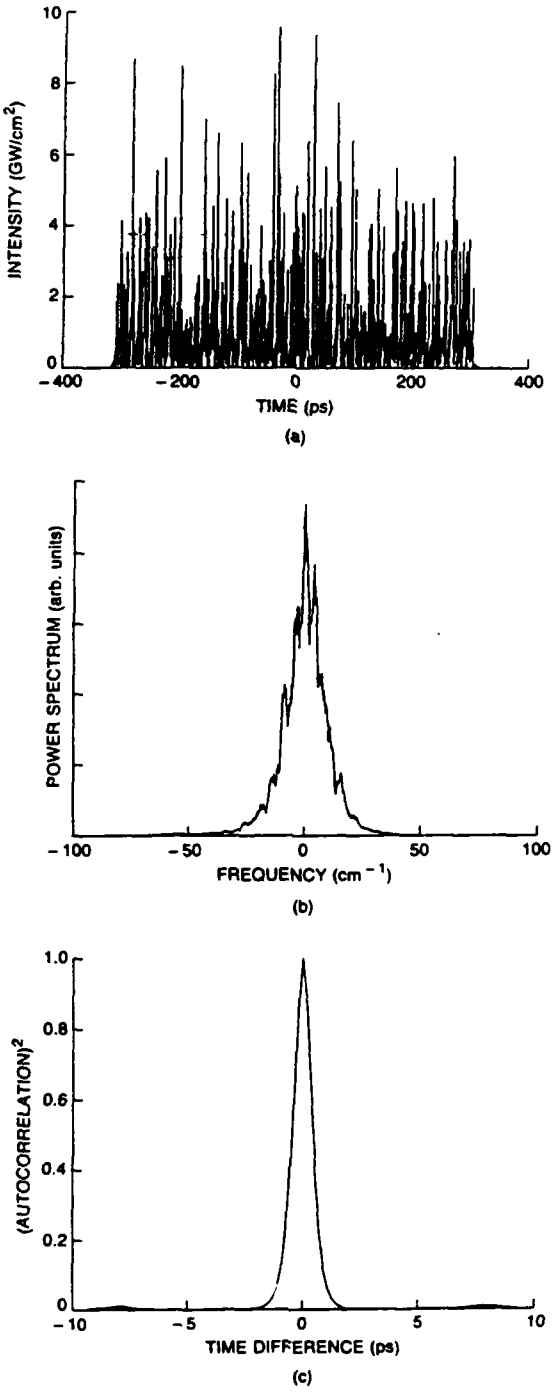

Fig. 2. Simulations of the incident fundamental light (1.054 μm), showing (a) the stochastic temporal behavior (average intensity is 1 GW/cm^2), (b) the power spectrum, and (c) the squared autocorrelation function.

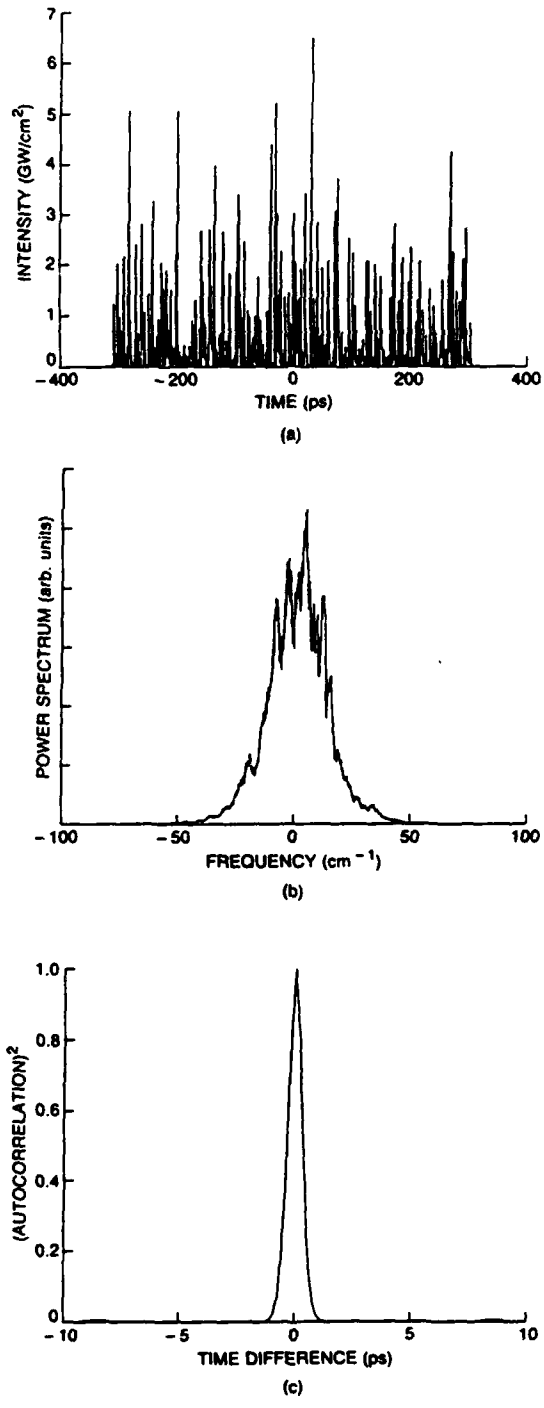

Fig. 3. Simulations of the second harmonic light generated in the first crystal, showing (a) the stochastic temporal behavior, (b) the power spectrum, and (c) the squared autocorrelation function.

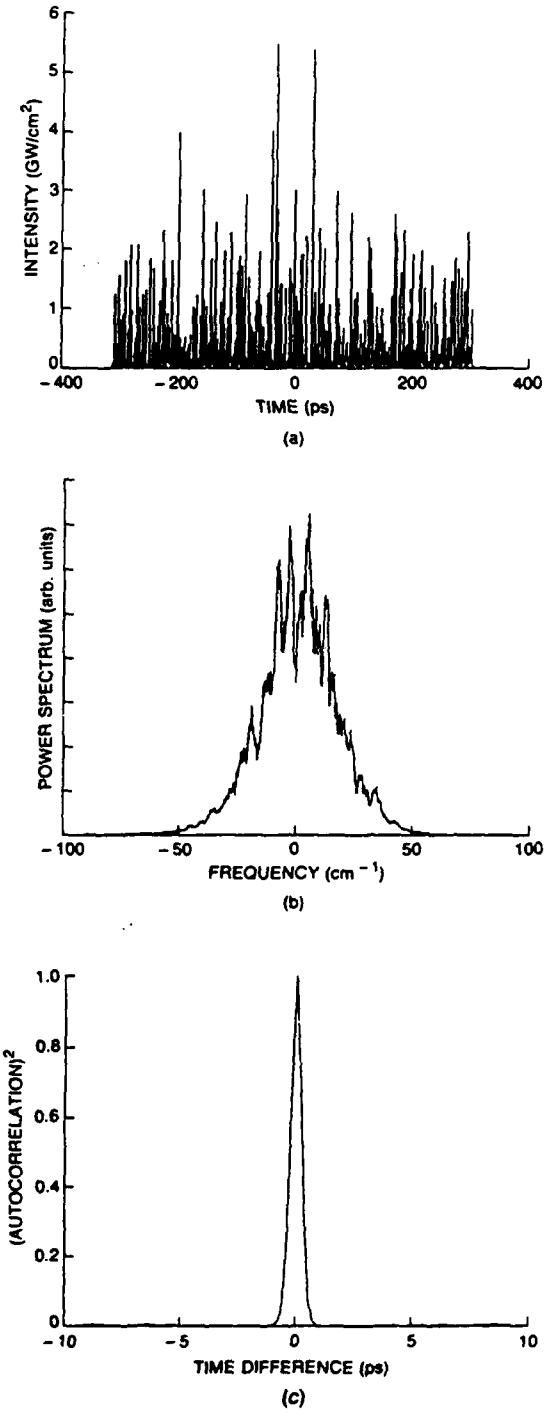

Fig. 4. Simulations of the second harmonic light generated in the second crystal, showing (a) the stochastic temporal behavior, (b) the power spectrum, and (c) the squared autocorrelation function.

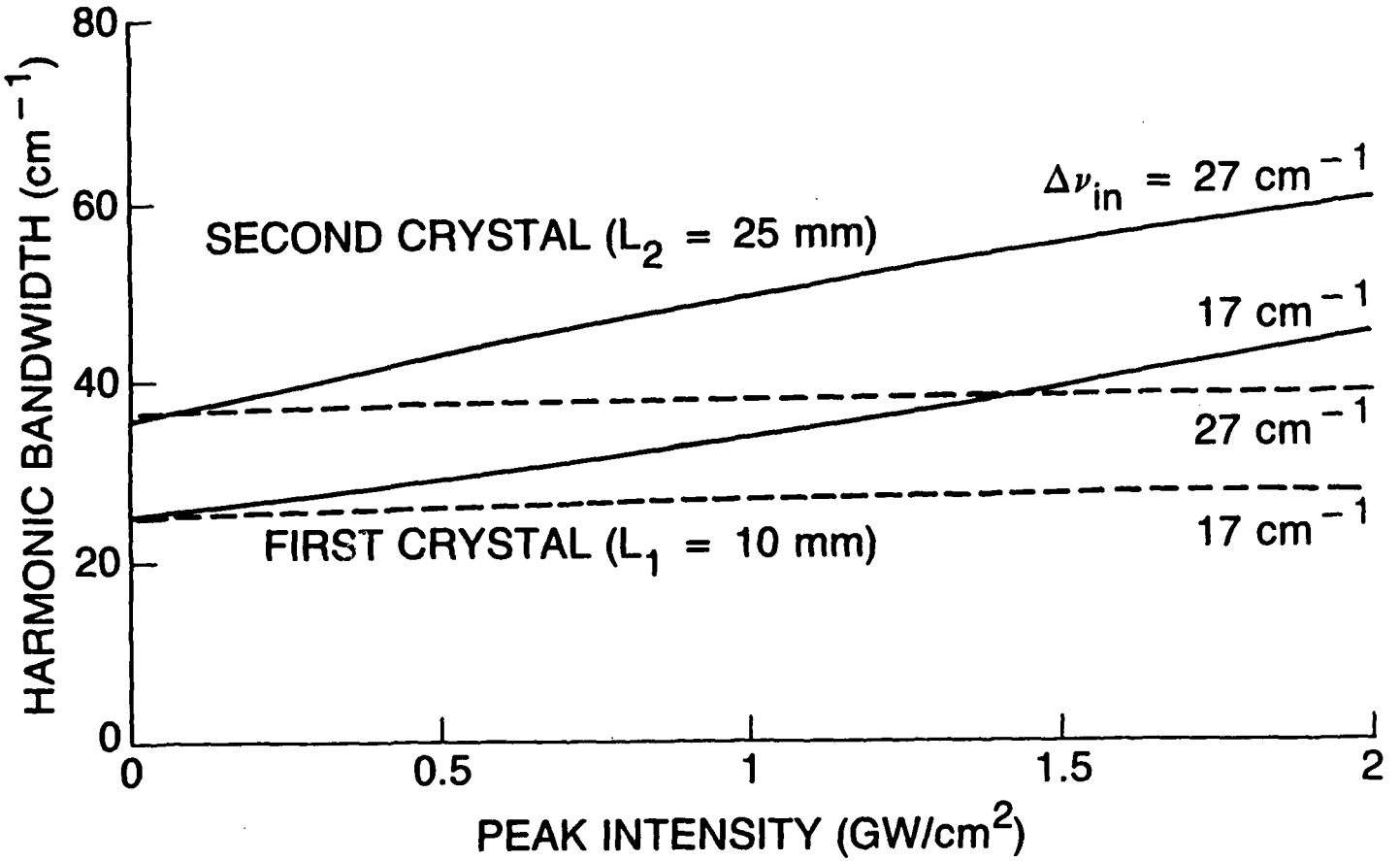

Fig. 5. Calculated bandwidths of the harmonic light generated in the first and second crystals (dashed and solid lines, respectively) vs. the average intensity of the incident fundamental at two different bandwidths.

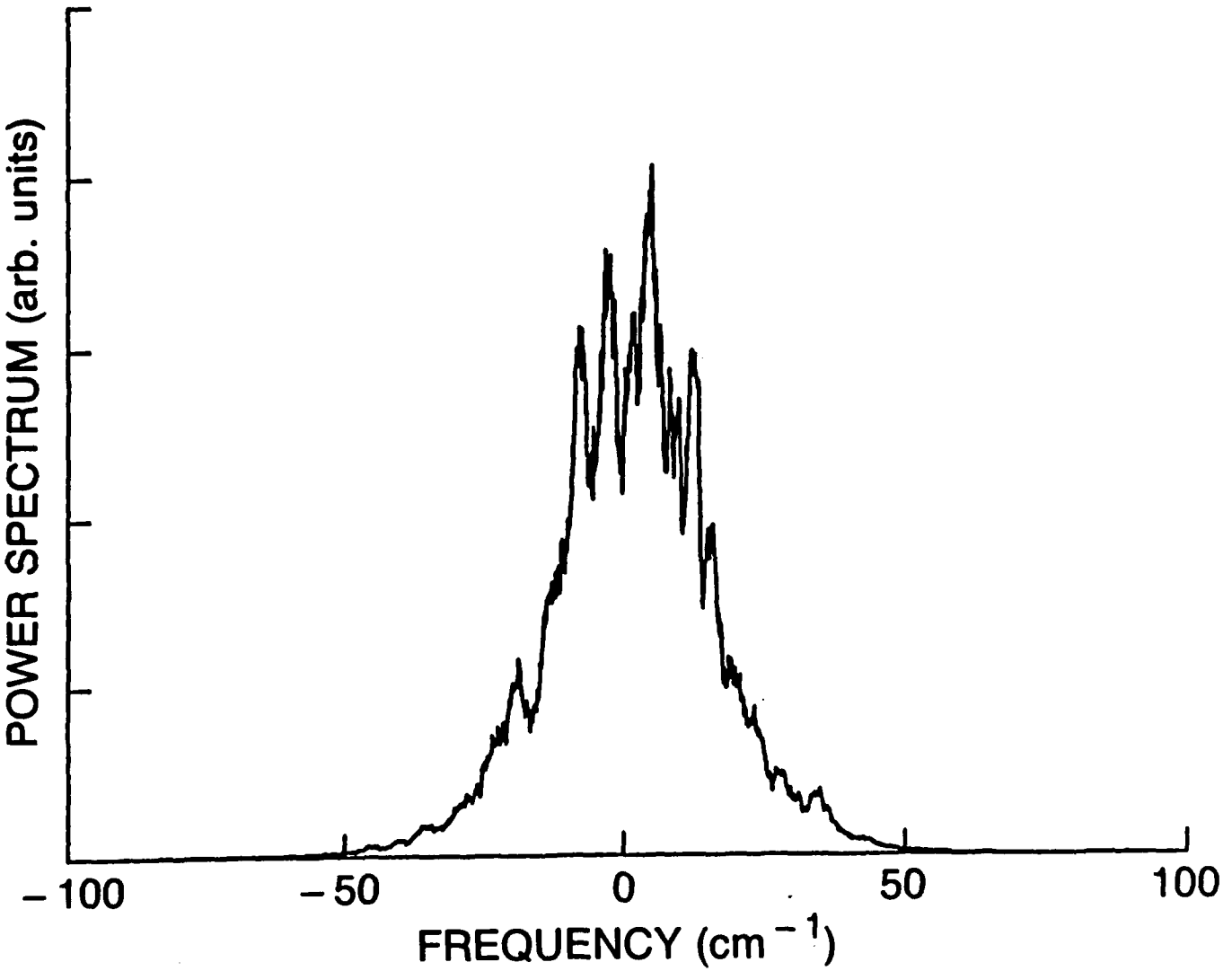

Fig. 6. Calculated spectrum of the total second harmonic light generated by two crystals in quadrature for an incident fundamental with an average intensity of 1 GW/cm^2 and a bandwidth of 17 cm^{-1}.

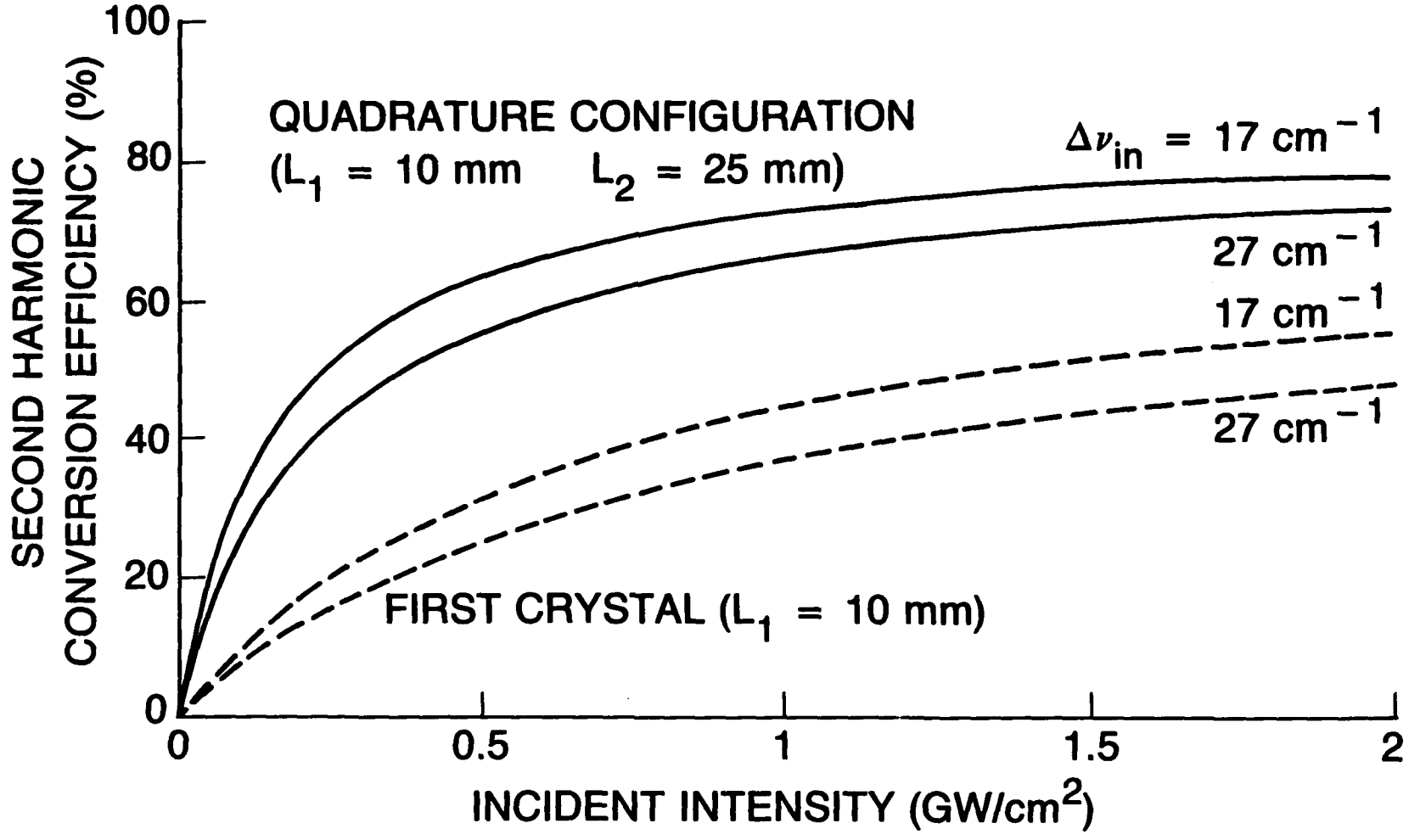

Fig. 7. Calculated second harmonic conversion efficiencies vs. average intensity of the incident fundamental at two different bandwidths. The dashed lines describe the harmonic conversion in the first crystal, while the solid lines describe the total harmonic conversion.

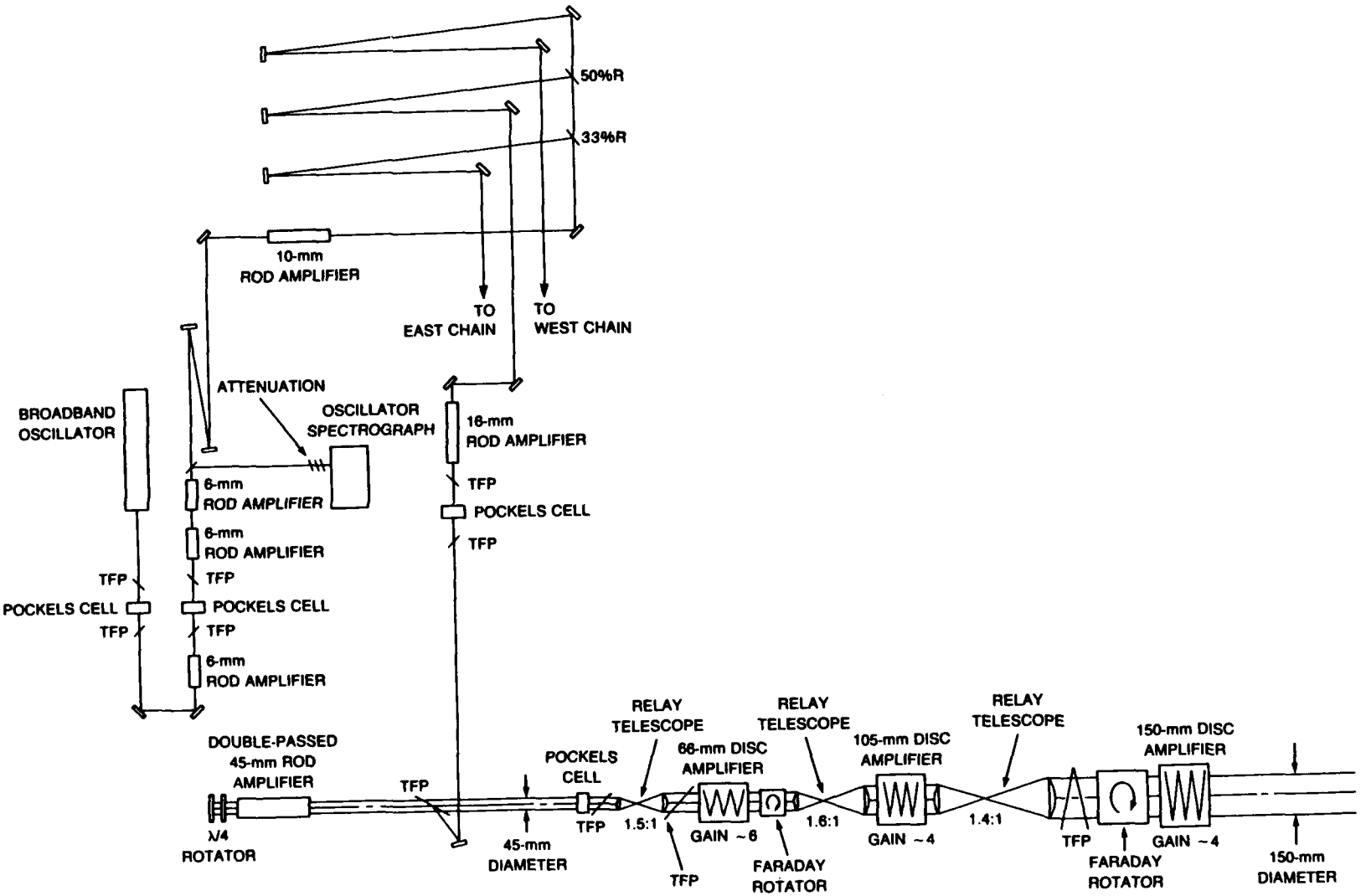

Fig. 8. PHAROS III Nd:Glass laser system. Alignment optics and some image relaying optics have been omitted for clarity. (TFP: Thin film polarizer)

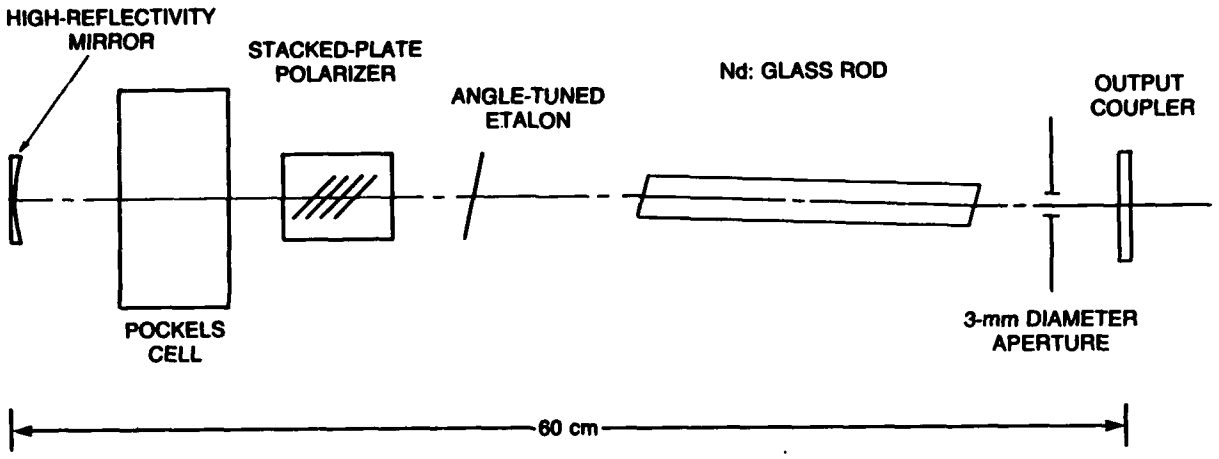

Fig. 9. Nd:Glass oscillator used to produce variable bandwidth laser spectrum.

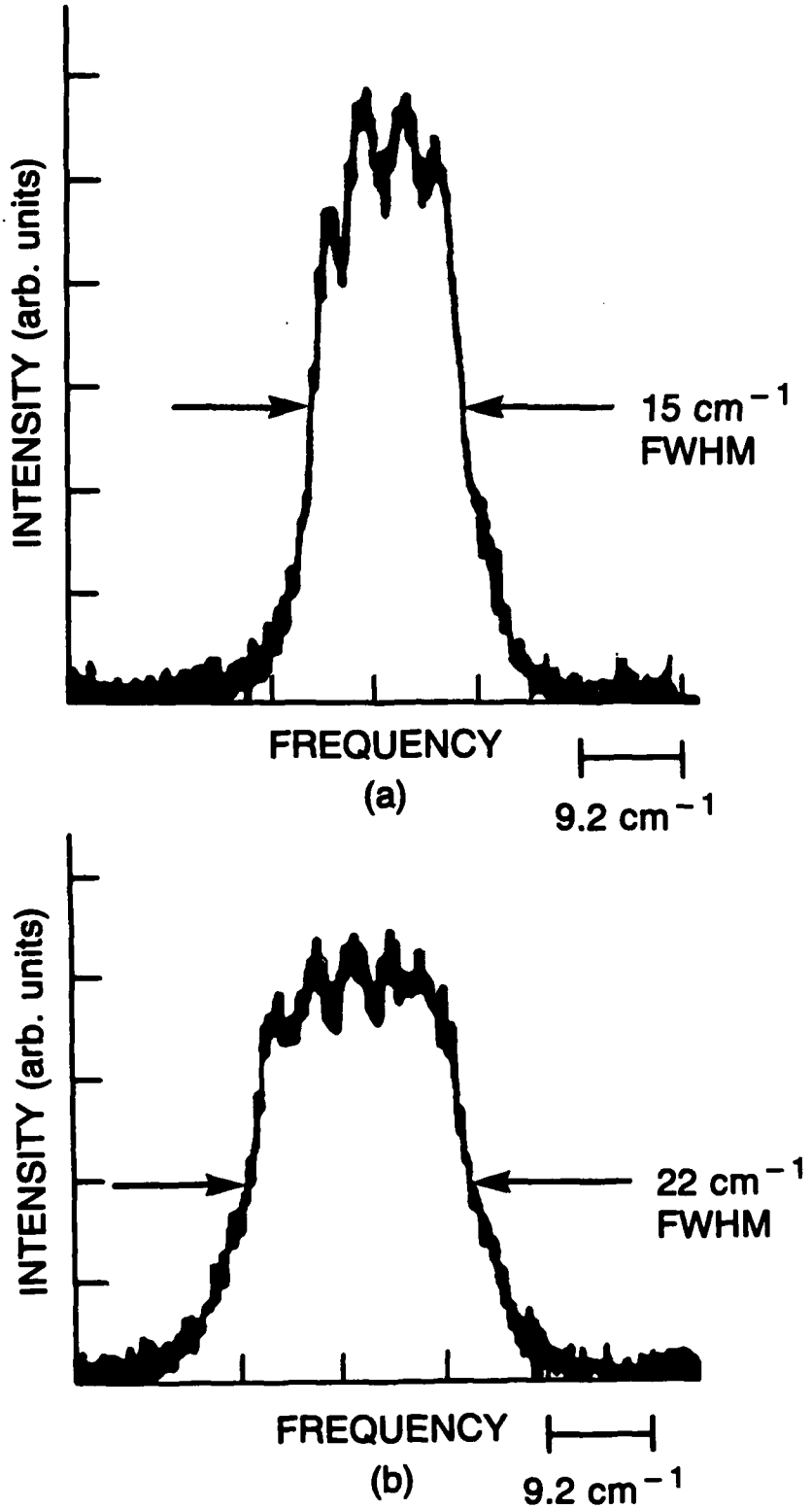

Fig. 10. Typical time-integrated oscillator spectra (center wavelength ~ 1.054 μm) for oscillator operation (a) without an intra-cavity etalon and (b) with an etalon.

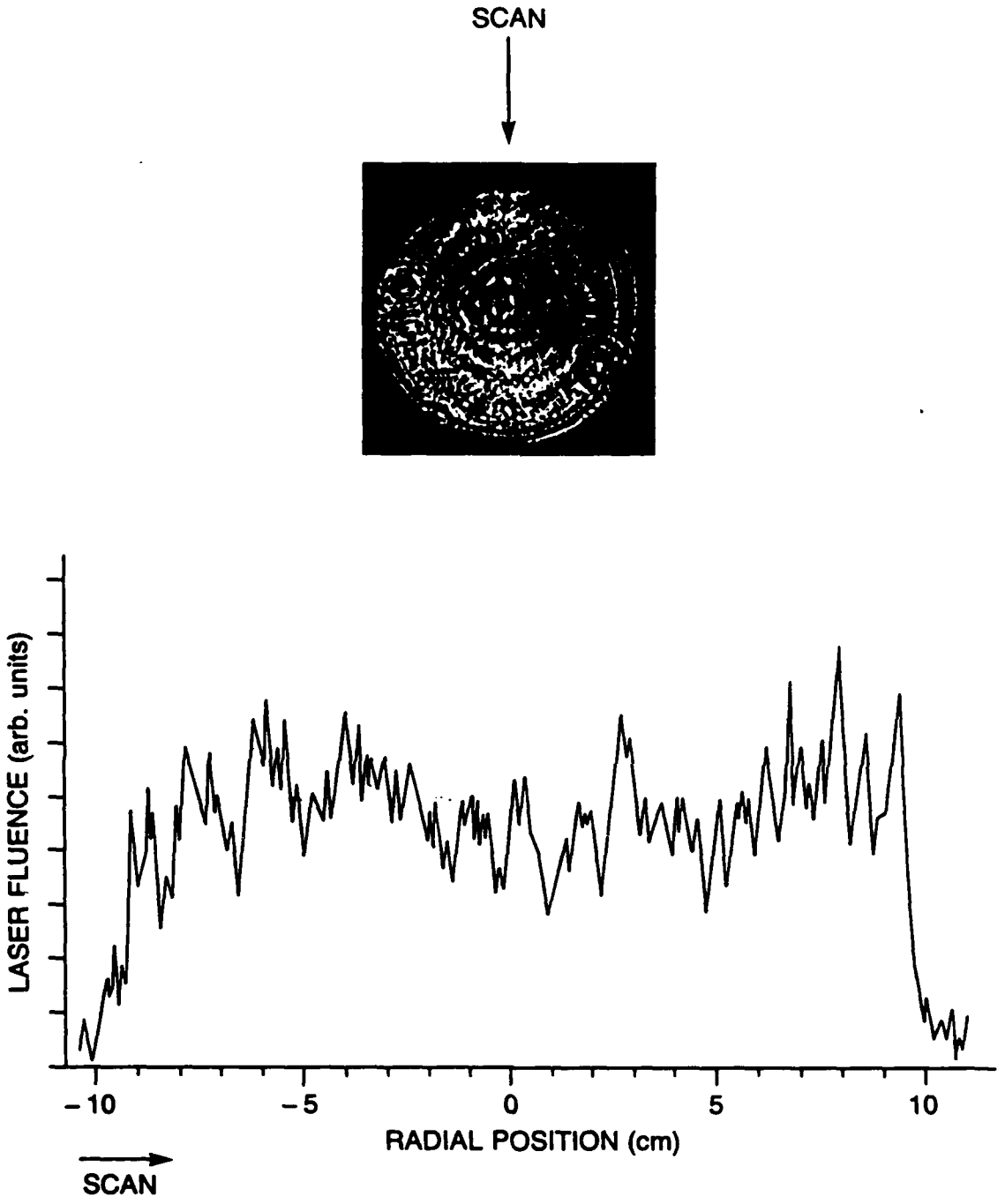

Fig. 11. Typical spatial profile and densitometer scan.

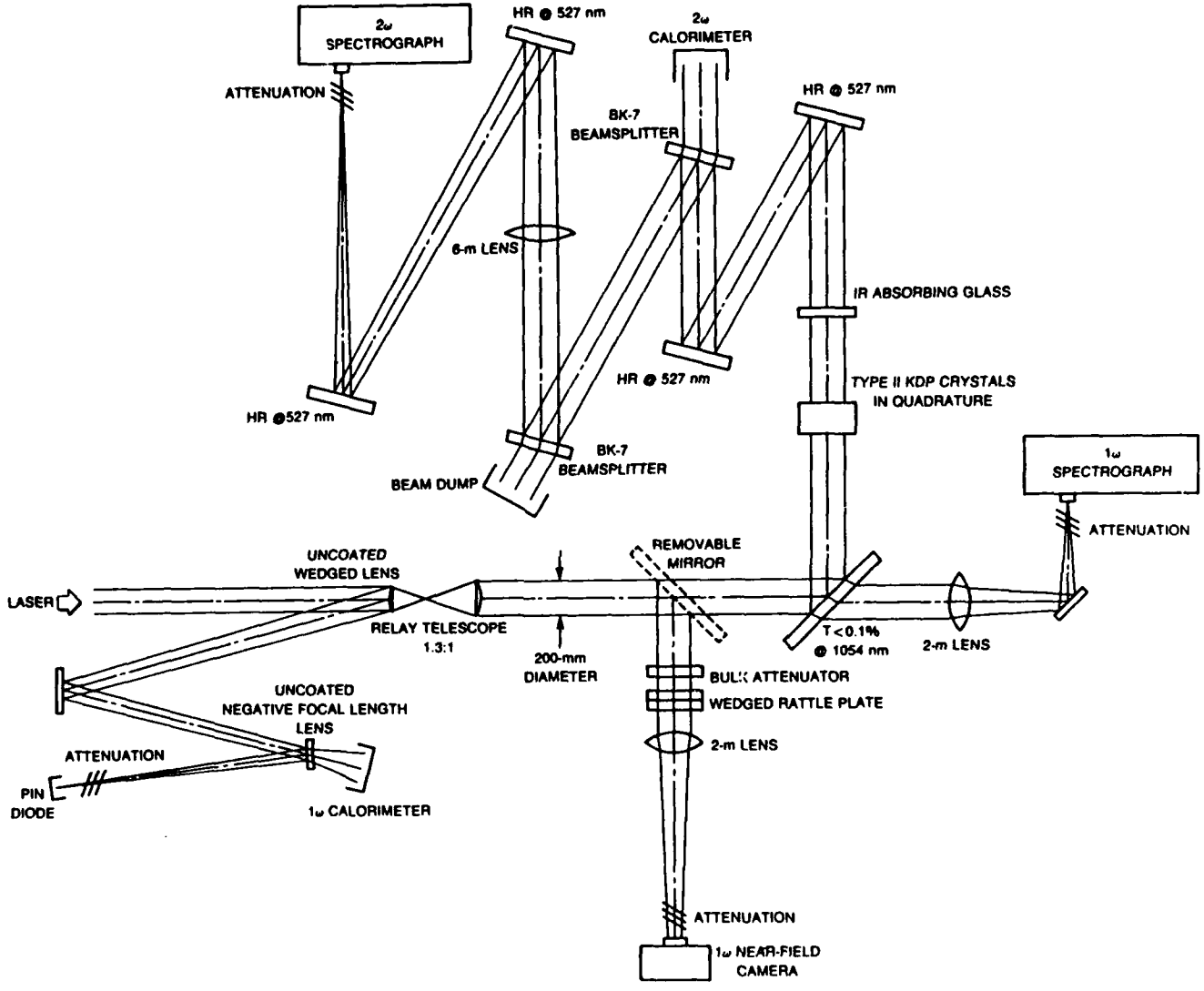

Fig. 12. Diagnostic arrangement used to measure the second harmonic conversion efficiency.

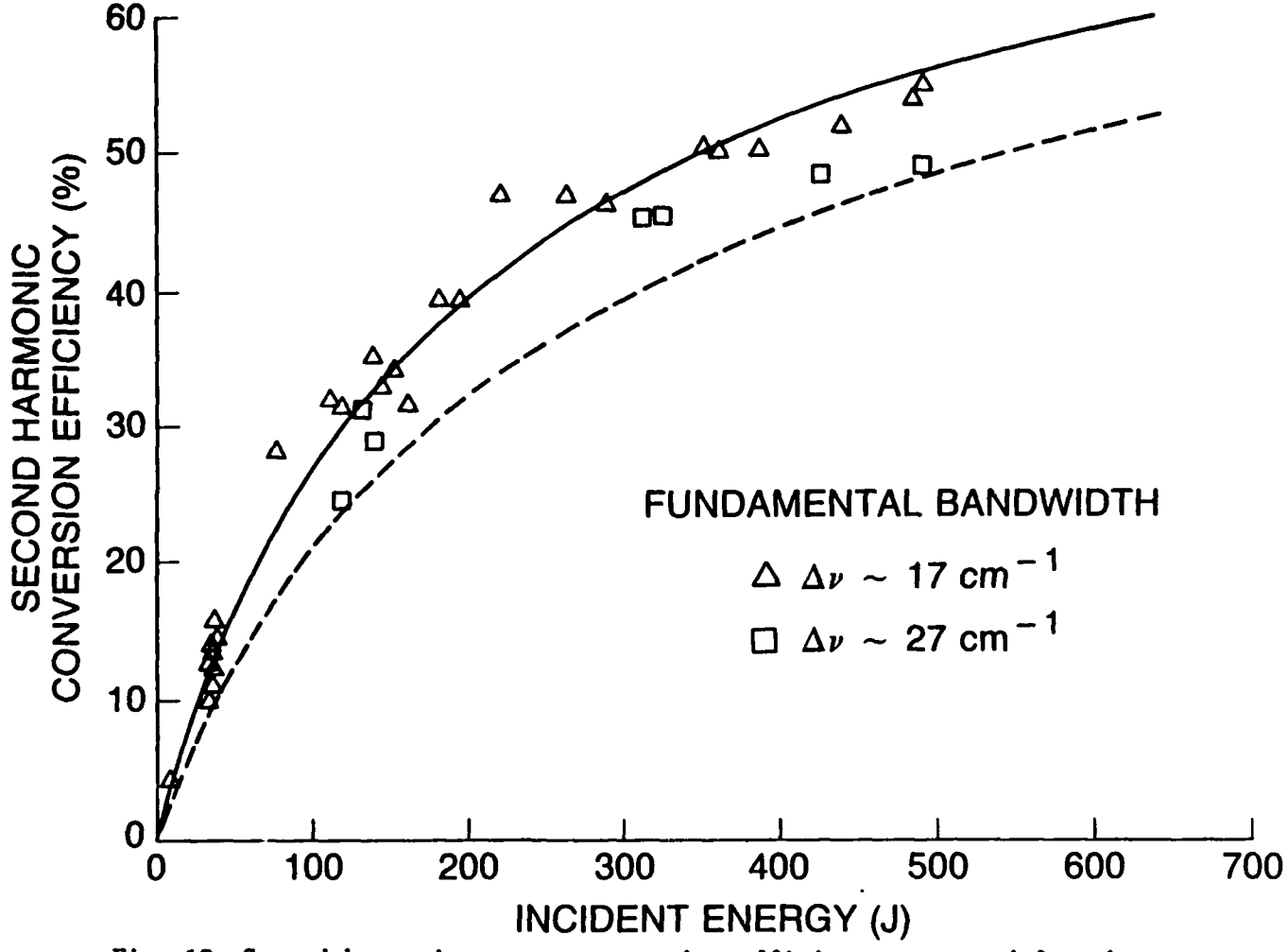

Fig. 13. Second harmonic energy conversion efficiency measured for the quadrature crystal arrangement. The theoretical predictions for fundamental FWHM bandwidths of 17 cm^{-1} and 27 cm^{-1} are shown as the solid and dashed lines, respectively. The peak intensity averaged across the beam was ~ 1 GW/cm^2 for a laser pulse energy of 500 J.

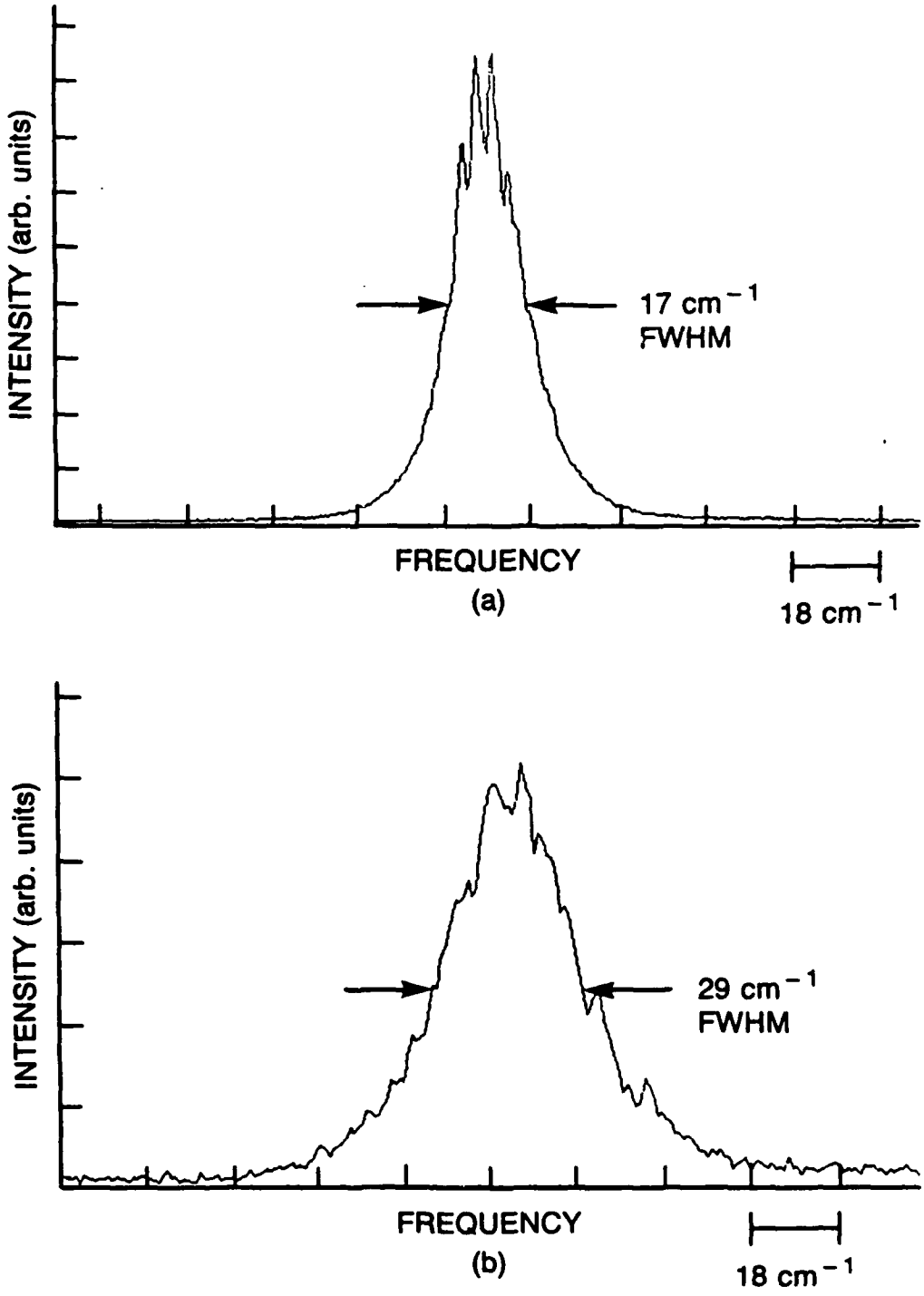

Fig. 14. Typical spectra for (a) the fundamental and (b) the second harmonic when no etalon is used in the oscillator.

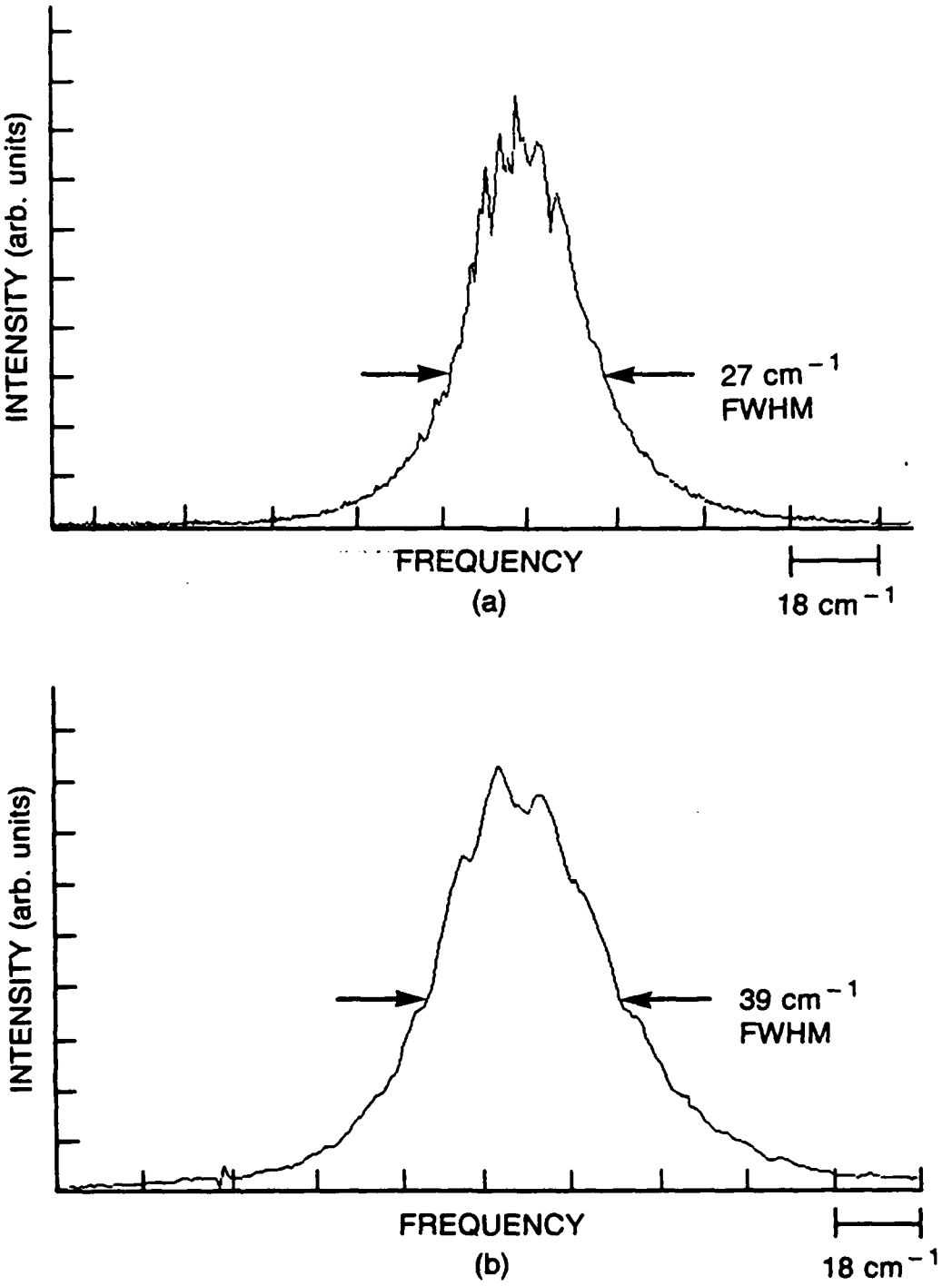

Fig. 15. Typical spectra for (a) the fundamental and (b) the second harmonic when an etalon is used in the oscillator to broaden the bandwidth.

DISTRIBUTION LIST

University of California
Lawrence Livermore National
Laboratory
P.O. Box 808
Livermore, CA 84550
R.L. Pond, L-302
J.L. Emmett, L-488
W.F. Krupke, L-488
J.F. Holzrichter, L-481
L.W. Coleman, L-473
J.T. Hunt, L-481
A.B. Langdon, L-477
I.F. Stowers, L-482

U.S. Dept. of Energy
Office of Inertial Fusion
Washington, D.C. 20545
M. Sluyter
C. Hilland
G. D'Alessio
S.L. Kahalas
J.E. Lewis
R.L. Schriever
T.H. Walsh

U.S. Dept. of Energy
Technical Information Center
P.O. Box 62
Oak Ridge, TN 37830

R. McCrory
University of Rochester
250 East River Road
Rochester, NY 14623

Robert T. Duff
U.S. Department of Energy
Office of Classification
Washington, D.C. 20545

Rex B. Purcell (2 cys.)
U.S. Department of Energy
Nevada Operations Office
P.O. Box 14100
Las Vegas, NV 89114 (136)

R. Bredderman
U.S. Department of Energy
San Francisco Operations
Office
1333 Broadway
Oakland, CA 94512

Los Alamos National Laboratory
P.O. Box 1663
Los Alamos, NM 87545
S.D. Rockwood, ICF Prog.
Mrg.
DAD/IF, MS 527 (2 cys.)

S. Bodner
Naval Research Laboratory
Code 4730
Washington, D.C. 20375

T. Coffey
Naval Research Laboratory
Code 1001
Washington, D.C. 20375

Alexander Glass
KMS Fusion, Inc.
3941 Research Park Drive
P.O. Box 1567
Ann Arbor, MI 48106

PaceVanDevenden (4 cys.)
Sandia National Laboratories
P.O. Box 5880
Albuquerque, NM 87185

Plasma Physics Division
Library
(Code 4730) - 25 copies

DIRECTOR OF RESEARCH
U.S. NAVAL ACADEMY
ANNAPOLIS, MD 21402
2 COPIES